ADVANCED MATERIALS
www.advmat.de

Engineered Surfaces That Promote Capture of Latent Proteins to Facilitate Integrin-Mediated Mechanical Activation of Growth Factors

Udesh Dhawan, Jonathan A. Williams, James F. C. Windmill, Peter Childs, Cristina Gonzalez-Garcia, Matthew J. Dalby, and Manuel Salmeron-Sanchez**

Conventional osteogenic platforms utilize active growth factors to repair bone defects that are extensive in size, but they can adversely affect patient health. Here, an unconventional osteogenic platform is reported that functions by promoting capture of inactive osteogenic growth factor molecules to the site of cell growth for subsequent integrin-mediated activation, using a recombinant fragment of latent transforming growth factor beta-binding protein-1 (rLTBP1). It is shown that rLTBP1 binds to the growth-factor- and integrin-binding domains of fibronectin on poly(ethyl acrylate) surfaces, which immobilizes rLTBP1 and promotes the binding of latency associated peptide (LAP), within which inactive transforming growth factor beta 1 (TGF-β1) is bound. rLTBP1 facilitates the interaction of LAP with integrin β1 and the subsequent mechanically driven release of TGF-β1 to stimulate canonical TGF-β1 signaling, activating osteogenic marker expression in vitro and complete regeneration of a critical-sized bone defect in vivo.

1. Introduction

The clinical utility of osteoinductive biomaterials for bone repair and regeneration is limited by adverse events such as postoperative inflammation, ectopic bone formation, and bone resorption[1–3] caused by the uncontrolled release of active growth factor molecules.[4,5] These challenges can be addressed by designing biomaterials that do not release active biomolecules but promote capture of growth factors onto an implant surface. This can be done by developing unconventional osteogenic biomaterials that exploit the physiological activation of growth factors by cell–extracellular matrix (ECM) interactions[6,7] to activate growth factors locally. This approach ensures that only those cells that have either adhered, or are in proximity, to the implant surface undergo osteogenic stimulation.

Fibronectin (FN) is a highly abundant ECM protein. It has crucial roles in maintaining cell adhesion and cell proliferation by enabling growth factor immobilization via its growth factor and integrin (ITG)-binding domains (FN_{12-14}).[8–12] FN is, therefore, routinely used as an intermediate coating on implants designed to immobilize growth factors such as transforming growth factor beta (TGF-β).[9,13] Recent studies have shown that TGF-β1 binds with greater affinity to FN's growth-factor-binding domain, relative to TGF-β2 or TGF-β3.[13] TGF-β1 is a well-studied growth factor that is essential for normal physiological functioning,[14,15] bone development,[16,17] and overall survival.[18] Although some studies report that TGF-β exerts osteoinhibitory effects, the nature of its observed effects depends on two key factors: the type of cell line[19–21] and the concentration of TGF-β used.[19,22] For instance, in C2C12 cells, TGF-β1 inhibition promotes osteogenic differentiation.[20] By contrast, in human mesenchymal stem cells (hMSCs), the cell line we use in this study, TGF-β1 activation promotes osteogenic differentiation.[22] Thus, although the indispensable role of TGF-β in osteogenic hMSC differentiation is well-established, its controlled use is essential for optimized bone regeneration.[23,24]

TGF-β1 is typically present in an inactive form that is trapped within latency associated peptide (LAP) via a disulfide bond. Its active form is released when LAP undergoes proteolytic degradation or interacts with integrins and latent-transforming growth

U. Dhawan, C. Gonzalez-Garcia, M. J. Dalby, M. Salmeron-Sanchez
Centre for the Cellular Microenvironment
Mazumdar-Shaw Advanced Research Centre
University of Glasgow
Glasgow G116EW, UK
E-mail: Udesh.Dhawan@glasgow.ac.uk;
Manuel.Salmeron-Sanchez@glasgow.ac.uk

J. A. Williams, P. Childs
Department of Biomedical Engineering
Wolfson Building
University of Strathclyde
Glasgow G4 0NW, UK

J. F. C. Windmill
Centre for Ultrasonic Engineering
Department of Electronic and Electrical Engineering
University of Strathclyde
Glasgow G11XW, UK

M. Salmeron-Sanchez
Institute for Bioengineering of Catalonia (IBEC)
The Barcelona Institute for Science and Technology (BIST)
Barcelona 08028, Spain

M. Salmeron-Sanchez
Institució Catalana de Recerca i Estudis Avançats (ICREA)
Barcelona 08010, Spain

The ORCID identification number(s) for the author(s) of this article can be found under https://doi.org/10.1002/adma.202310789

DOI: 10.1002/adma.202310789

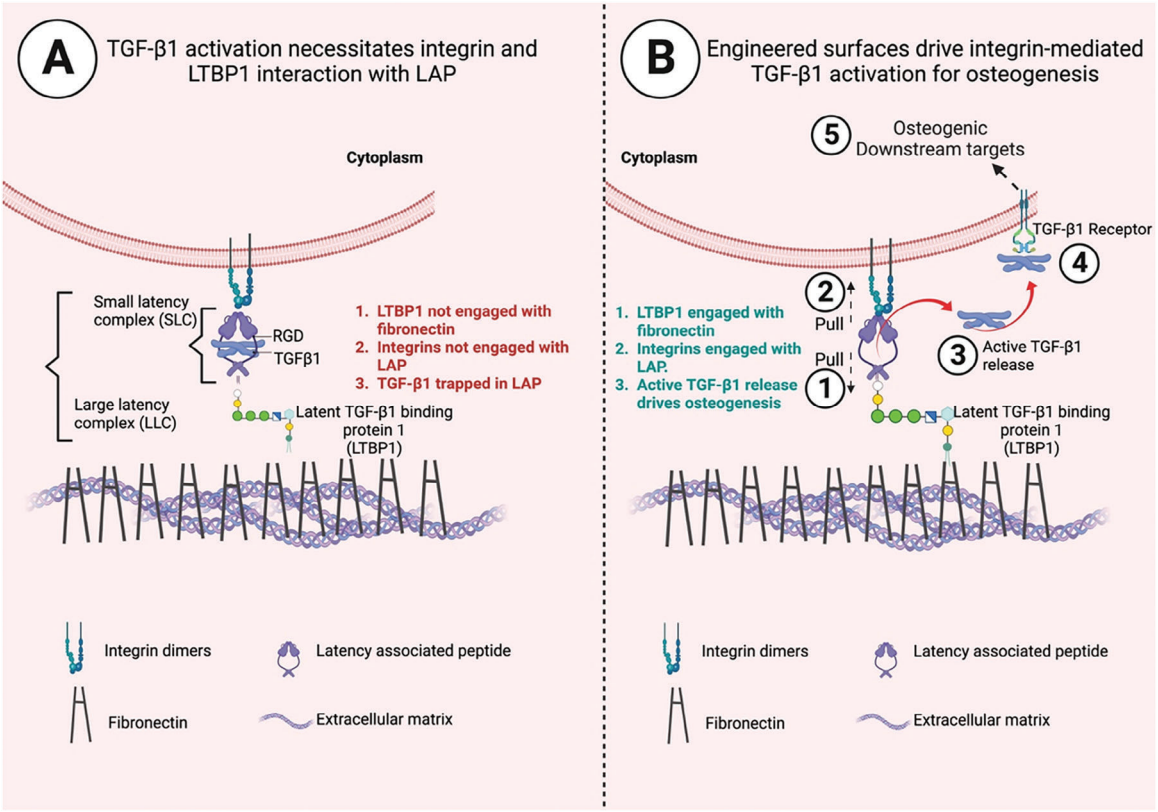

Scheme 1. A,B) Schematic of integrin- and LTBP-1-mediated release of TGF-β1. B. The mechanical pulling of LAP by integrins and by fibronectin-bound *LTBP1* triggers the mechanical release of TGF-β1 to activate osteogenic TGF-β1 signaling.

factor beta-binding protein-1 (*LTBP1*).[25–27] FN also plays an important role in TGF-β1 activation as it immobilizes *LTBP1*, which facilitates LAP binding and TGF-β1 activation.[28] We therefore hypothesized that the immobilization of *LTBP1* on FN-coated surfaces might promote capture of inactive, LAP-bound TGF-β1 to enable its controlled and site-specific integrin-mediated release. This unconventional approach, in which we utilize a latent protein, might help to address the deleterious, nonspecific effects of using active growth factors, as in conventional osteoinductive approaches. **Scheme 1** explains the rationale of using integrin and *LTBP1* to stimulate the mechanical release of TGF-β1.

In this study, we coated surfaces first with poly(ethyl acrylate) (PEA), a polymer that enhances the availability of FN growth-factor- and integrin-binding domains,[29,30] and then with FN to enable recombinant *LTBP1* (rLTBP1) immobilization. We hypothesized that this engineered surface will promote capture of inactive, LAP-bound TGF-β and facilitate the controlled and site-specific integrin-mediated mechanical release of TGF-β1 to activate the osteogenic TGF-β1 signaling pathway and stimulate bone regeneration.

2. Results

2.1. Characterization of PEA, FN, and rLTBP1 Coatings

We have previously shown that plasma-polymerized PEA increases the availability of the $FNIII_{9–10}$ and $FNIII_{12–14}$ domains of plasma FN, thereby promoting growth factor immobilization and synergistic integrin–growth factor receptor interactions.[29,30] In this study, we used PEA to immobilize rLTBP1 peptide to stimulate osteoinduction.

We coated standard polystyrene culture plates with PEA using plasma polymerization. The chemical structure of polystyrene (uncoated tissue culture plates) and PEA is shown in **Figure 1A**. We performed X-ray photoelectron spectroscopy (XPS) to confirm PEA coating on polystyrene surfaces. Carbon spectra of polystyrene surfaces showed C═C moieties at 284.4 eV, whereas PEA-coated surfaces showed O—C═O moieties at 288.9 eV (Figure 1B). In addition, while oxygen spectra of uncoated surfaces showed C—O moieties at 532.8 eV potentially from plasma treatment of polystyrene tissue culture plates, PEA-coated surfaces showed C═O moieties at 532.1 eV (Figure 1C). These carbon and oxygen spectra confirmed the successful coating of PEA on polystyrene surfaces.

FN adopts a globular molecular arrangement on uncoated polystyrene surfaces that transforms into nanonetworks on PEA-coated surfaces.[31] This change increases the exposure of the $FNIII_{9–10}$ and $FNIII_{12–14}$ domains that are responsible for integrin- and growth-factor binding, respectively.[30] We confirmed by atomic force microscopy (AFM, Figure 1D) and by scanning electron microscopy (SEM, Figure 1E and Figure S1A (Supporting Information)) that FN formed nanonetworks on PEA surfaces. We then investigated if PEA-coated surfaces promoted higher FN adsorption as compared to uncoated

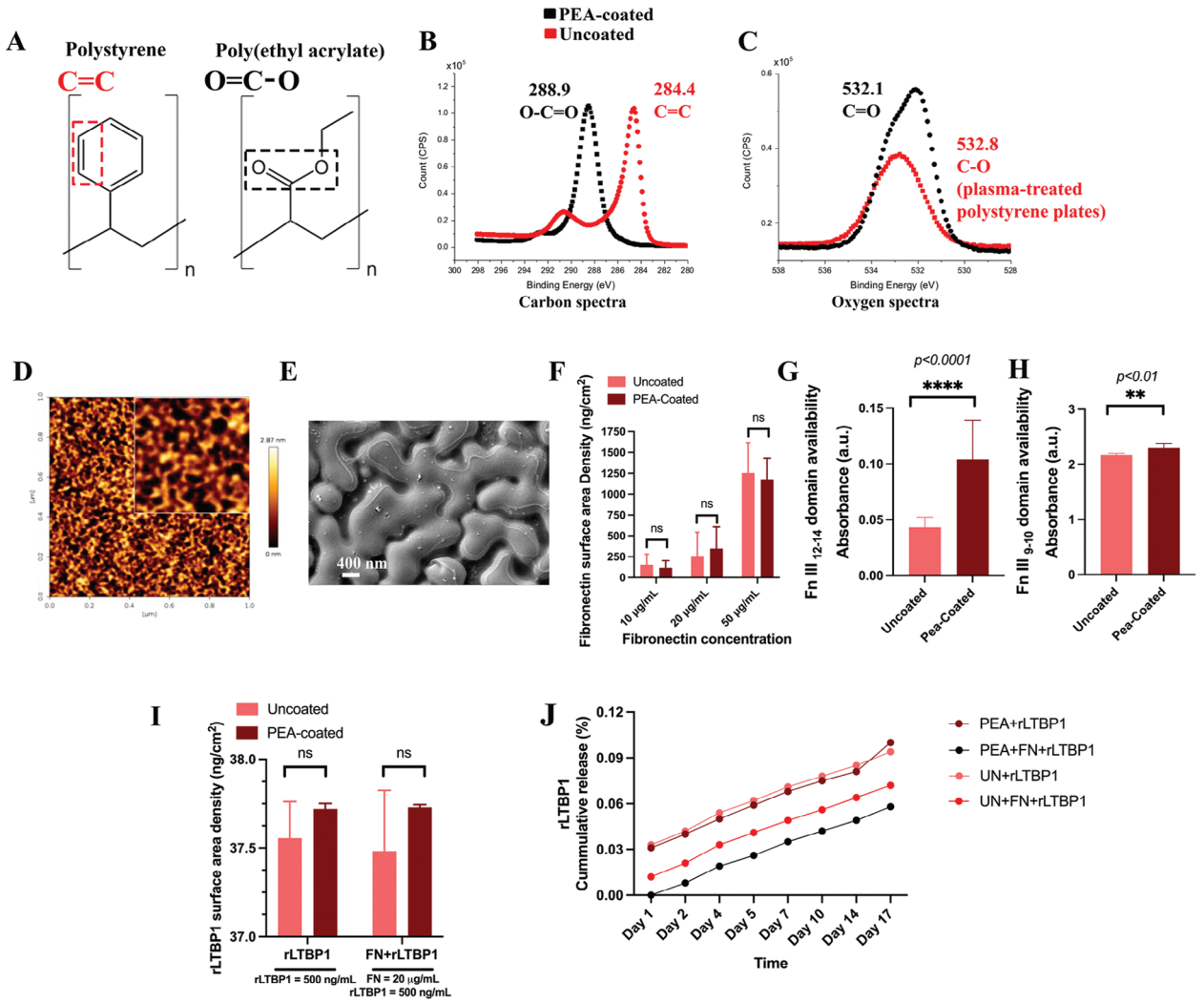

Figure 1. Characterization of poly(ethyl acrylate), fibronectin, and rLTBP1 coatings. A) Chemical structure of polystyrene and poly(ethyl acrylate) (PEA). B,C) XPS characterization of polystyrene and PEA-coated polystyrene surfaces. Carbon and oxygen spectra confirm the coating of PEA on polystyrene surface. D) AFM characterization of FN nanonetworks formed on PEA-coated surface. Inset shows an enlarged version of a small section within the image. E) Scanning electron microscopy (SEM) of FN coating on PEA-coated surface. SEM image shows the formation of FN nanonetworks. Scale bar = 400 nm. F) Amount of FN adsorbed on uncoated and PEA-coated surface as measured using micro-BCA protein quantification assay. Significant difference in the surface area density of FN on uncoated and PEA-coated surfaces was not observed (n = 3, Shapiro–Wilk normality test, followed by two-way ANOVA with Sidak's multiple comparison test). G) Comparison of FN growth-factor-binding domain availability on uncoated and PEA-coated surfaces as measured using ELISA. Growth-factor-binding domain was significantly more abundant on PEA-coated, relative to uncoated, surfaces (n = 9, Shapiro–Wilk normality test, followed by Mann–Whitney test). H) Comparison of FN integrin-binding (RGD) domain availability on uncoated and PEA-coated surfaces as measured using ELISA. PEA-coated surfaces resulted in higher abundance of FN RGD domain, relative to uncoated surfaces (n = 9, Dixon's Q test to identify any outlier, Shapiro–Wilk normality test, followed by an unpaired t-test with Welch's correction). I) Quantification of rLTBP1 amount adsorbed on uncoated+FN or PEA+FN-coated surfaces using ELISA (n = 3, Shapiro–Wilk normality test, followed by two-way ANOVA with Tukey's multiple comparison test). J) Quantification of temporal release profile of rLTBP1 on uncoated, PEA-coated, uncoated+FN, or PEA+FN surfaces using ELISA. For statistical analysis of all quantitative data, first Shapiro–Wilk normality test was performed to assess if data displayed normal distribution. Parametric tests were employed to compare datasets that displayed normal distribution, whereas nonparametric tests were employed to compare datasets that did not display normal distribution.

surfaces (polystyrene plates). We quantified the amount of FN adsorbed on PEA and uncoated surfaces using micro-BCA (Bicinchoninic. acid assay) protein assay, but found no significant differences in FN surface area density (Figure 1F). However, interestingly, assessment of $FNIII_{9–10}$ and $FNIII_{12–14}$ domain availability using enzyme-linked immunosorbent assay (ELISA) revealed that PEA-coated surfaces induced a higher availability of $FNIII_{9–10}$ and $FNIII_{12–14}$ domains, compared to uncoated surfaces (Figure 1G,H). Because FN surface area density on uncoated and PEA-coated surfaces was similar, the higher

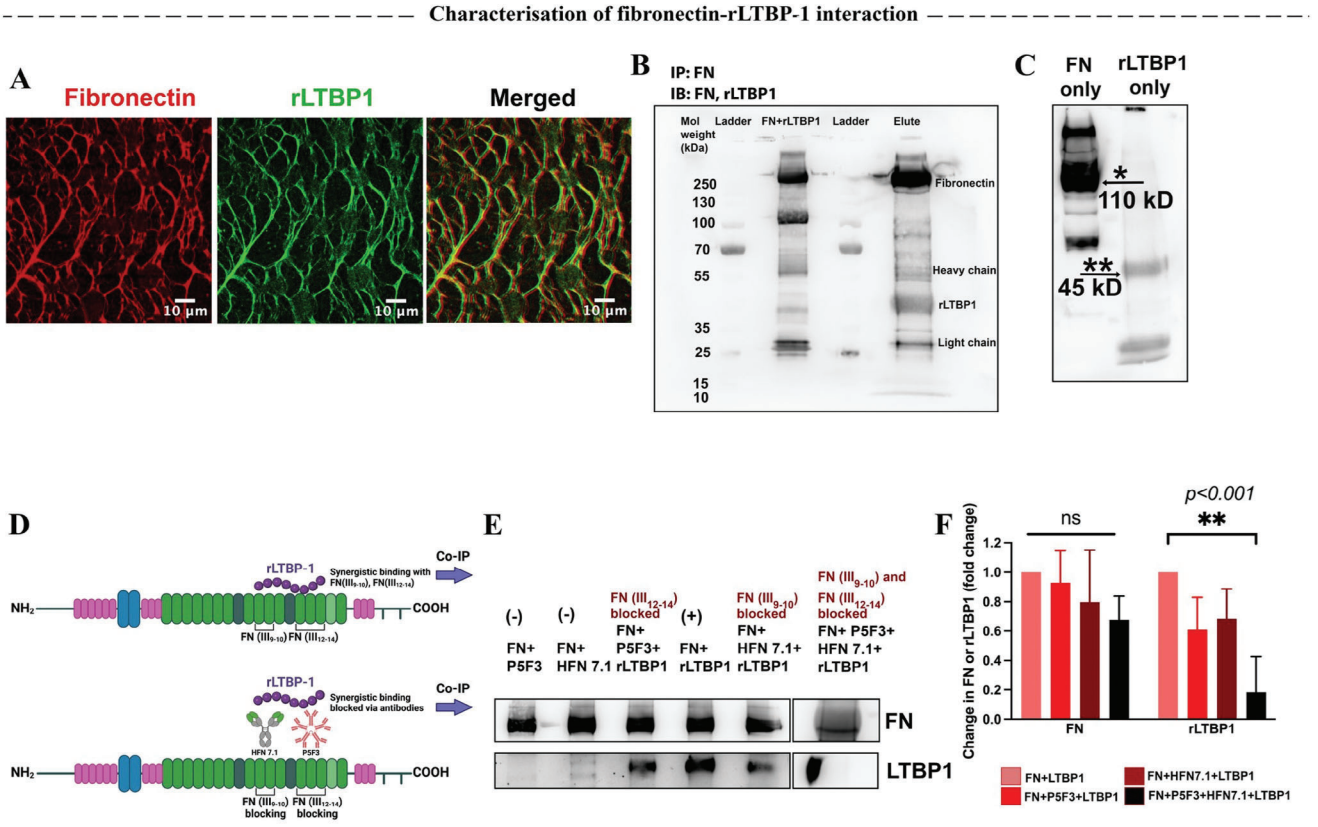

Figure 2. rLTBP1 binds with plasma fibronectin (FN) by interacting with growth-factor- and integrin-binding domains. A) Immunolabeling images of FN and rLTBP1 on PEA-coated surfaces, showing colocalization and likely interaction of FN and rLTBP1. Scale bar = 10 µm. B) Characterization of FN+rLTBP1 interaction by coimmunoprecipitation. The mixture of FN and rLTBP1 was incubated with anti-FN antibodies and immunoblots were probed using FN and *LTBP1* antibodies. Both antibodies were raised in different species. rLTBP1 was present at validated molecular weight of 44 kDa. FN+rLTBP1 fraction failed to bind to bead–antibody complex and was referred to as elute. C) Western blotting of FN and rLTBP1 when run separately to characterize their molecular weight and identify the corresponding protein bands. D) Schematic of experimental design used to evaluate rLTBP1 binding with FN growth factor and RGD domain. Growth-factor-binding and integrin-binding FN domains were blocked using P5F3 and HFN7.1 antibodies, respectively. E) Coimmunoprecipitation was performed to evaluate decrease in rLTBP1 binding with FN when growth-factor- and integrin-binding domains were blocked. The mixture of FN and rLTBP1 was incubated with antibodies against growth factor and integrin-binding domains (P5F3 and HFN7.1, respectively). Immunoblotting was then performed and blots were probed for FN and rLTBP1. FN and rLTBP1 mixture without blocking antibodies was used as a positive control. Beads alone and FN antibody alone were used as negative controls. F) Quantitative analysis of decrease in rLTBP1 binding with FN upon growth-factor- and integrin-binding domain blocking ($n = 3$, Shapiro–Wilk normality test, followed by two-way ANOVA test with Šidák multiple comparison test). Densitometric analysis was performed using ImageJ to quantify protein band intensity. We observed a significant decrease in rLTBP1 binding to FN when FN's growth factor and integrin binding domains were both blocked. For statistical analysis of all quantitative data, first Shapiro–Wilk normality test was performed to assess if data displayed normal distribution. Parametric tests were employed to compare datasets that displayed normal distribution, whereas nonparametric tests were employed to compare datasets that did not display normal distribution.

abundance of $FNIII_{9–10}$ and $FNIII_{12–14}$ domains on PEA-coated surfaces can be attributed to FN's organization as nanonetworks. Thus, nanonetwork formation is a crucial step as it promotes the exposure of FN's integrin- and growth-factor-binding domains.

We then characterized rLTBP1 adsorption on uncoated or PEA-coated surfaces with/without FN using ELISA and observed that the presence of PEA and/or FN did not significantly increase the amount of rLTBP1 adsorbed (Figure 1I). Interestingly, rLTBP1 surface area density on uncoated+rLTBP1 and uncoated+FN+rLTBP1 was identical (37.4 ng cm^{-1}), indicating that FN's presence had no effect on the amount of rLTBP1 adsorbed. We made a similar observation when comparing rLTBP1 density on PEA+rLTBP1 with PEA+FN+rLTBP1 as both surfaces displayed identical rLTBP1 density (37.7 ng cm^{-1}, Figure 1I). We then tested the temporal stability of rLTBP1 coating on uncoated/PEA-coated surfaces with/without FN (Figure 1J). We observed rLTBP1 coating to be remarkably stable on all surfaces, with <0.15% of rLTBP1 released over two weeks. However, <0.05% of rLTBP1 coating was released on PEA+FN surfaces over 2 weeks, and rLTBP1 release was twofold lower after 2 weeks on this surface compared to PEA alone. FN might thus improve rLTBP1's stability (Figure 1J). This observation prompted the need to evaluate FN+rLTBP1 interaction on PEA surfaces.

We observed via immunolabeling that FN and rLTBP1 colocalized on PEA surfaces, indicating that they interact (**Figure** 2A). By translating the mass of FN and rLBTP1 adsorbed to the number of molecules, we were able to calculate their stoichiometries. We found that FN and rLTBP1 exhibited a 0.93:1 stoichiometry, i.e., 1 molecule of rLTBP1 possibly interacts with 0.93 (precisely)

molecules of FN. We next investigated FN and rLTBP1 interactions by immunoprecipitation. We incubated the mixture of FN and rLTBP1 proteins with anti-FN antibody and hypothesized that the presence of rLTBP1 on immunoblots would imply interaction between FN and rLTBP1. We found that rLTBP1 coimmunoprecipitated with FN (Figure 2B). We performed western blotting of both proteins separately to characterize their molecular weights via the corresponding protein bands (Figure 2C). To identify the precise FN domains responsible for rLTBP1 binding, we blocked $FNIII_{9-10}$ and $FNIII_{12-14}$ domains using monoclonal antibodies (Figure 2D), immunoprecipitated FN, and probed for FN and rLTBP1. P5F3 and HFN7.1 antibodies alone, and FN+P5F3 and FN+HFN7.1 groups without rLTBP1 were used as negative controls (Figure 2D,E and Figures S1C,D and S2 (Supporting Information)). On blocking FN growth-factor-binding (with P5F3) and integrin-binding (with HFN7.1) domains, we observed that rLTBP1 binding to FN reduced by 40% and 32%, respectively (Figure 2F), and that blocking both domains resulted in 82% decrease in rLTBP1 binding (Figure 2F). This observation is plausible as the entire FNIII domain is 90 amino acids long; by contrast, the rLTBP1 peptide used here is 297 amino acids long, and as such could interact with both growth-factor- and integrin-binding domains. Collectively, these findings confirm that rLTBP1 interacts with FN via growth factor and integrin-binding domains.

2.2. *LTBP1* Immobilizes LAP and Facilitates Integrin-Mediated TGF-β Release

Having confirmed the interaction between rLTBP1 and FN, we next identified the rLTBP1 concentration that elicits optimal TGF-β and osteogenic biomarker response. We performed quantitative real-time polymerase chain reaction (RT-qPCR) and observed that *TGFB1* gene expression increased consistently until rLTBP1 concentration reached 500 ng mL^{-1} and then dropped below control level at 1 µg mL^{-1} concentration (**Figure 3A**). *BGLAP* (bone gamma-carboxyglutamate protein, osteocalcin) gene expression showed a similar trend; its expression was the highest at 500 ng mL^{-1} rLTBP1 concentration (Figure 3B) and dropped to 1.4-fold at 1 µg mL^{-1} concentration. We observed similar trends in osteopontin and *Runx-2* gene expression (Figure S3A, Supporting Information). Collectively, these results show that a 500 ng mL^{-1} concentration of rLTBP1 produces the highest TGF-β activation.

Pioneering work by Klingberg et al. has shown that ectodomain-A (ED-A) of cellular fibronectin (cFN) is crucial for *LTBP1* accumulation in the ECM[9] (here, we refer to plasma and cellular fibronectin as pFN and cFN, respectively, for ease of distinction). To evaluate whether cFN presents rLTBP1 more efficiently than pFN, we assessed *TGFB1* gene expression on cFN and pFN-coated surfaces. We also investigated whether mouse- and human-derived rLTBP1 activated *TGFB1* gene to different extents. First, we coated surfaces with PEA and then with pFN or cFN, and finally with mouse- or human-derived rLTBP1. We then evaluated the activation of TGF-β1 by measuring change in *TGFB1* gene transcript levels and its downstream osteogenic targets using RT-qPCR. Contrary to our expectations, we obtained the highest levels of *TGFB1*, *BGLAP*, and osteopontin (*OPN*) gene expression in cells cultured on PEA surfaces coated with pFN and mouse-derived rLTBP1 [ms(rLTBP1), Figure 3C and Figure S3B (Supporting Information)]. This result was intriguing because pFN lacks ED-A, the widely accepted scaffold for *LTBP1*,[9,28] yet this combination produced the highest *TGFB1* gene expression. By contrast, cFN combined with (ms)rLTBP1 produced the lowest *TGFB1* gene expression response. (ms)rLTBP1 on PEA surfaces without any FN coating failed to stimulate *TGFB1* gene expression. Thus, we observed a *TGFB1* gene response only when FN was present, despite rLTBP1 having a similar surface area density on both PEA+rLTBP1 and PEA+FN+rLTBP1 surfaces (Figure 1I). These results indicate that FN is needed for efficient rLTBP1 presentation and that pFN on PEA with (ms)rLTBP1 elicits the highest *TGFB1* gene response.

We next assessed whether rLTBP1 immobilization stimulates full-length *LTBP1* secretion to result in TGF-β1 activation. We first assessed *LTBP1* gene and protein expression on PEA-coated/uncoated surfaces using RT-qPCR and western blotting, respectively. The PEA+FN+rLTBP1 coating produced the highest *LTBP1* gene (1.5-fold) and protein expression (20-fold increase, Figure 2D,G). We note that *LTBP1* probed via western blotting is full-length and not the one presented on the surface (rLTBP1, 45 kDa) owing to its molecular weight (>250 kDa). We propose that full-length *LTBP1* is deposited in the ECM to regulate TGF-β1 expression (Figure 2E,G). The PEA+FN+*LTBP1* coating resulted in the highest FN expression of any of the tested protein–peptide combinations on PEA or uncoated surfaces (Figure 2E,F and Figure S3C (Supporting Information)). We propose that these increased FN levels are deposited in the ECM and immobilize full-length *LTBP1* for TGF-β1 activation.

Physiologically, FN immobilizes *LTBP1*, which then interacts with LAP to facilitate TGF-β1 activation (as schematized in Figure 3H). To assess this possible interaction, we performed colocalization experiments. We immunolabeled FN and *LTBP1* to study their colocalization and found that cells cultured on PEA surfaces displayed little FN or *LTBP1* staining in the ECM (Figure 3I). By contrast, cells cultured on PEA+FN+*LTBP1* surfaces displayed distinct FN/*LTBP1* colocalization in the ECM (Figure 3J). These results confirm that FN/*LTBP1* interacts on PEA surfaces, which is vital for immobilizing LAP and for subsequent TGF-β1 release.

The peptide-mediated release of TGF-β1 requires *LTBP1* to immobilize LAP, thereby allowing integrins to bind LAP's RGD (Arginylglycylaspartic acid) sequence (Figure 3K).[26,32] We therefore investigated the *LTBP1*–LAP interaction by immunoprecipitation. We incubated total protein lysates from PEA or PEA+FN+rLTBP1 experimental groups with LAP antibodies (VB3A9) and probed for LAP and *LTBP1*. Our results showed that higher levels of *LTBP1* coimmunoprecipitated with LAP on PEA+FN+*LTBP1* surfaces than on PEA control surfaces, confirming an enhanced *LTBP1*–LAP interaction (Figure 3L and Figure S4 (Supporting Information)). We further validated this interaction by immunostaining *LTBP1*/LAP and assessing their colocalization (Figure 3M). We immunolabeled our results confirming that on PEA+FN+*LTBP1* surfaces, *LTBP1*–LAP interactions are enhanced, demonstrating the second step in TGF-β1 release from LAP.

Integrin β-subunit is known to be crucial for the release of TGF-β from LAP (Figure 3N).[33,34] Gene and protein expression

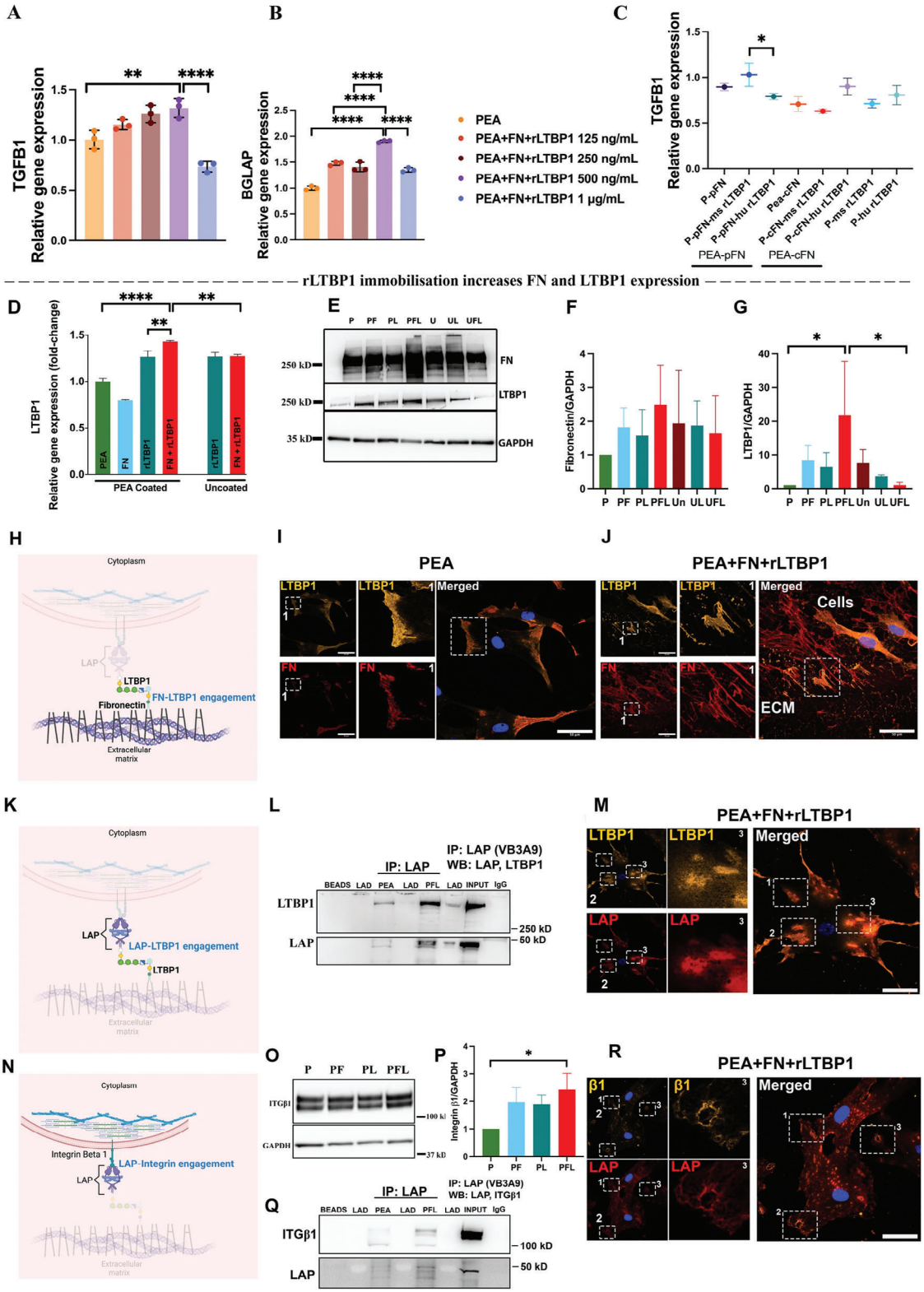

Figure 3. Mechanism of TGF-β1 activation. A,B) RT-qPCR analysis of *TGFB1* and *BGLAP* (osteocalcin) gene transcript levels in response to varying concentrations of rLTBP1($n = 3$, Shapiro–Wilk normality test, followed by one-way ANOVA with Tukey's multiple comparison test, * and ** denoted $p \leq 0.05$ and 0.01, respectively, and **** denoted $p \leq 0.0001$). Substrates coated with rLTBP1 at 500 ng mL^{-1} dosage displayed the highest *TGFB1* and *BGLAP* gene expression in cells. Gene expression on different surfaces was normalized to that on PEA-only coated surfaces. C) RT-qPCR analysis of *TGFB1* gene transcript levels after PEA-coated substrates were coated with plasma or cellular fibronectin followed by coating with human or mouse

analysis using RT-qPCR and western blotting, respectively, revealed that cells on PEA+FN+rLTBP1 surfaces expressed high levels of integrin β1 (Figure 3O,P and Figure S5 (Supporting Information)). This increase is attributed to the presence of rLTBP1 because cells with or without FN (PEA+FN or PEA+rLTBP1) displayed similar protein levels of integrin β1 (Figure 3P and Figure S6 (Supporting Information)). We then performed coimmunoprecipitation by incubating total protein lysates from PEA and PEA+FN+rLTBP1 experimental groups with ITGβ1 antibodies followed by probing using ITGβ1 and LAP antibodies. Coimmunoprecipitation revealed higher levels of β1 immunoprecipitated with LAP on PEA+FN+rLTBP1 than on PEA surfaces (Figure 3Q and Figure S6 (Supporting Information)), confirming that the FN+rLTBP1 coating promoted integrin β1 and LAP interaction. We further verified this interaction by performing colocalization experiments by immunolabeling ITGβ1 and LAP using antibodies raised in different species (Figure 3R). From these results, we propose that LAP's interaction with *LTBP1* and integrin β1 facilitates TGF-β1 release on PEA+FN+rLTBP1 surfaces.

2.3. rLTBP1-Mediated TGF-β Activation Drives Osteogenesis

Figure 4A,B shows the steps leading to TGF-β signaling pathway activation. To investigate this, we immunolabeled TGF-β1 and TGF-βRI using antibodies raised in different species, and assayed for ligand–receptor interaction via colocalization. On PEA+FN+rLTBP1 surfaces, we observed numerous areas of TGF-β1 and TGF-βRI colocalization, indicating that TGF-β1 released from LAP interacts with TGF-βRI (Figure 4C). By western blotting, we found that the PEA+FN+rLTBP1 combination resulted in a 12-fold increase in active TGF-β1 expression, relative to PEA control group (Figure 4D). TGF-β1 knockdown by small interfering RNA (siRNA) targeting *TGFB1* gene resulted in 1.4-fold lower expression (Figure 4D and Figure S7 (Supporting Information)). We note that relative to control (PEA only) surfaces, cells on all surfaces produced higher levels of active TGF-β1, likely due to rLTBP1 being adsorbed onto all surfaces. Nevertheless, this result shows that the FN coating of PEA surfaces is important for presenting rLTBP1 for optimal TGF-β1 activation. Noteworthy, the inclusion of uncoated, uncoated+rLTBP1, and uncoated+FN+rLTBP1 experimental groups also revealed lower TGF-β1 protein expression than on PEA+FN+rLTBP1, confirming that the combination of PEA with FN and rLTBP1 is essential for eliciting the highest TGF-β1 protein expression in cells.

We then studied the protein expression of suppressor of mothers against decapentaplegic (Smad) 2 and 3 via western blotting. Phosphorylated Smad 2/3 (p-Smad2/3) displayed a similar trend in protein levels as seen with TGF-β1 (Figure 4E and Figure S7 (Supporting Information)). TGF-β1 knockdown by siRNA decreased phosphorylated Smad2/3 levels confirming its efficacy in inhibiting the propagation of TGF-β1 signaling pathway (Figure 4E). The nuclear translocation of total and phosphorylated Smad2/3 was also enhanced, confirming TGF-β1 signaling activation (Figure S8A, Supporting Information).

To confirm that TGF-β1 activation is mechanically driven by integrins, we used Rock inhibitor (Y-27632) to regulate cell contractility. Rock inhibition resulted in disruption of stress fiber filaments, as visualized by the immunolabeling of F-actin and phosphorylated myosin light chain-2 (p-MLC2, Figure 4F), diminishing the cells' ability to pull on the ECM. Rock inhibition was validated by western blotting, which showed a decrease in phosphorylated MLC2 and myosin phosphatase subunit 1 (p-MYPT1, Figure 4H). To assess if Rock inhibition disrupted integrin β1/LAP interaction and the release of active TGF-β1, we investigated the colocalization of immunolabeled integrin β1 and LAP via immunostaining. Rock inhibition disrupted their colocalization (Figure 4G) as observed via immunostaining, and western blotting revealed a corresponding decrease in active TGF-β1 (25 kDa) protein expression (Figure 4I). These experiments confirm the involvement of integrin β1 in the mechanical release of TGF-β1 and in subsequent TGF-β1 signaling pathway activation.

We then evaluated the osteogenic potential of PEA+FN+rLTBP1 surfaces over time using RT-qPCR. After day 7 on PEA+FN+rLTBP1 surfaces, cells showed the highest gene expression levels of osteogenic markers *BGLAP*, *OPN*, and *Runx-2*, relative to surfaces only coated with PEA (Figure 4J). These genes showed decreased expression following TGF-β1 knockdown by siRNA, confirming their regulation by TGF-β1, and lower gene expression levels on uncoated surfaces,

rLTBP1 ($n = 3$, Shapiro–Wilk normality test, followed by Kruskal–Wallis test with Dunn's multiple comparisons test, * denotes $p \leq 0.05$). Gene expression on different surfaces was normalized to that on PEA-only coated surfaces. The combination of plasma fibronectin with mouse rLTBP1 resulted in the highest *TGFB1* gene level in cells. Abbreviations – P: PEA, ms: mouse, hu: human, pFN: plasma fibronectin, cFN: cellular fibronectin. D) RT-qPCR analysis of *LTBP1* gene transcript levels ($n = 3$, Shapiro–Wilk normality test, followed by one-way ANOVA with Tukey's multiple comparison test) on different substrates. rLTBP1 immobilization on FN resulted in the highest *LTBP1* gene expression. Gene expression on different surfaces was normalized to that on PEA-only coated surfaces. E) Immunoblots showing FN and *LTBP1* protein expression. F,G) Quantitative analysis of FN and *LTBP1* protein expression levels using densitometric analysis on ImageJ ($n = 3$, Shapiro–Wilk normality test, followed by one-way ANOVA with Tukey's multiple comparison test). Explanation of abbreviations – P: PEA, F: Fibronectin, L: *LTBP1*, Un: Uncoated. GAPDH was used as a housekeeping gene and PEA was used as a reference sample. H) Schematic representation of FN+rLTBP1 interaction. I) Immunofluorescence staining of *LTBP1* and fibronectin showing their colocalization in cells but not in the ECM on PEA surfaces. J) Immunofluorescence staining of *LTBP1* and FN showing their colocalization in the cells and ECM. ECM is represented in the dotted rectangle next to cells. Scale bar = 50 µm. K) Schematic representation of *LTBP1*–LAP interaction. L) Immunoblots confirming LAP and *LTBP1* interaction. LAP was immunoprecipitated, and LAP and *LTBP1* probed for by western blotting. *LTBP1*'s presence confirmed its interaction with LAP. Beads only and LAP antibody only were used as negative controls. M) Immunofluorescence staining of *LTBP1* and LAP showing their interaction via colocalization. Scale bar = 50 µm. N) Schematic representation of integrin β1–LAP interaction, an important step in TGF-β1 release from LAP. O) Immunoblots showing integrin β1 protein levels. P) Quantitative analysis of integrin β1 protein levels using densitometric analysis in ImageJ. GAPDH was used as a housekeeping gene and PEA as reference samples ($n = 3$, Shapiro–Wilk normality test, followed by one-way ANOVA with Tukey's multiple comparison test)). Q) Immunoblots confirming integrin β1 and LAP interaction. LAP was immunoprecipitated, and LAP and integrin β1 probed by western blotting. Integrin β1's presence confirmed its interaction with LAP. Beads only and LAP antibody only were used as negative controls. R) Immunofluorescence staining of *LTBP1* and LAP showing numerous areas of their interaction assessed via colocalization. Scale bar = 50 µm.

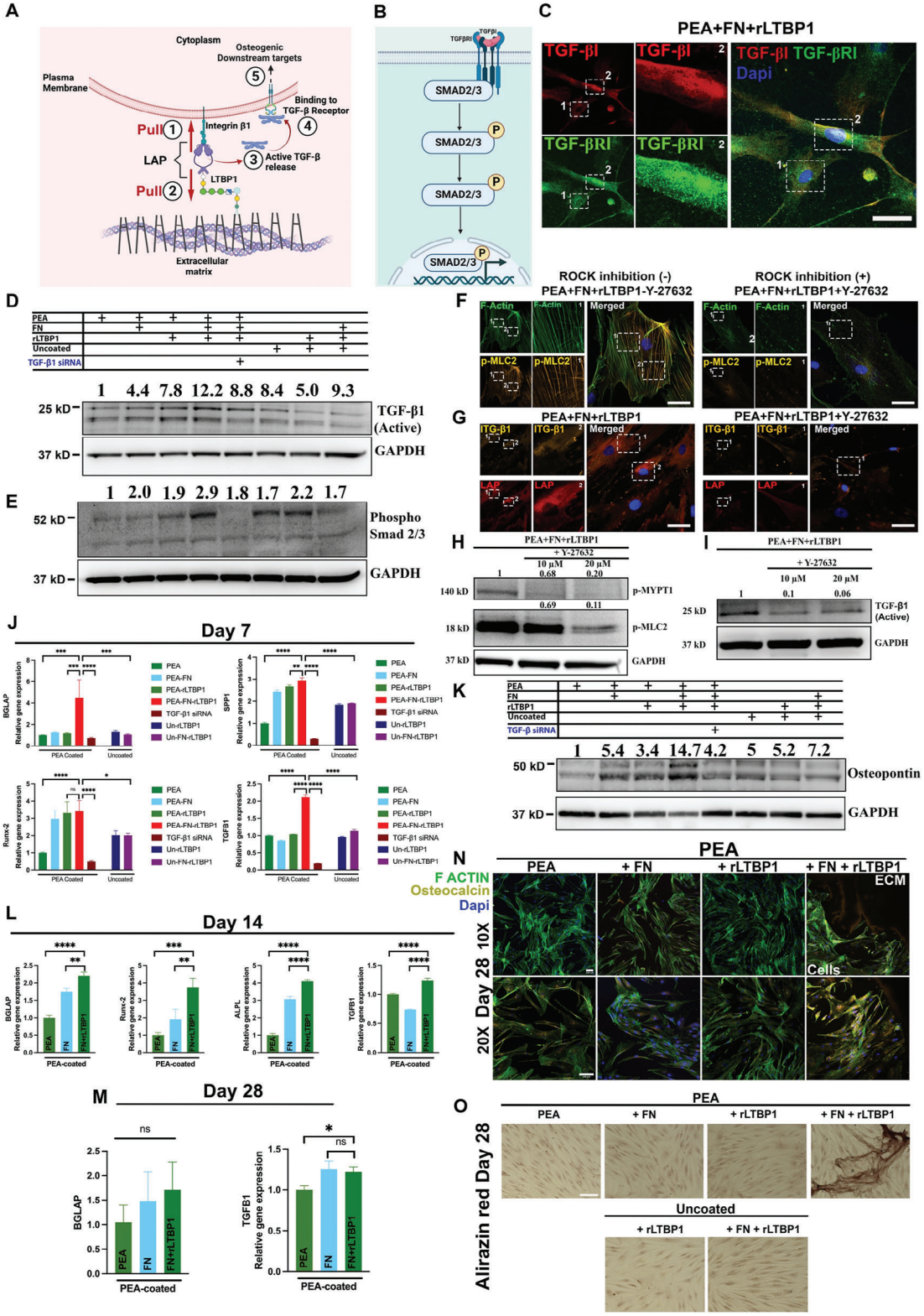

Figure 4. TGF-β1 activation drives osteogenesis. A) Schematic of TGF-β1 activation. Integrin β1 and *LTBP1* interact with either side of LAP, resulting in TGF-β1's mechanical release. B) Schematic of the TGF-β1 signaling pathway. TGF-β1 binds to its receptor (TGF-βRI) to activate canonical TGF-β signaling pathway. C) Immunofluorescence staining of TGF-β1 and TGF-βRI. (TGF-βRI originally stained with Alexa Fluor 568 but changed to a green color for ease of visualization). Colocalization areas are highlighted with dashed rectangles. Scale bar = 50 μm. D) Immunoblots showing active TGF-β1 homodimer levels at 25 kDa. GAPDH was used as a loading control. The highest TGF-β1 levels, which decreased upon siRNA-mediated knockdown,

highlighting the role of PEA. Osteopontin protein levels as assessed via western blotting after day 7 complemented the gene expression results (Figure 4K and Figure S8B (Supporting Information)). On PEA+FN+rLTBP1, *BGLAP*, *Runx-2*, and *ALP* (Alkaline phosphatase) gene expression remained the highest after day 14 relative to other surfaces (Figure 4L), with *BGLAP* expression being the highest after day 28 (Figure 4M). By contrast, protein expression assessed using western blotting was found to be the highest on PEA only surfaces than on PEA+FN+rLTBP1 surfaces (Figure S9, Supporting Information). To investigate whether this discrepancy is due to western blotting measuring protein levels only in cells, we immunolabeled osteocalcin to see if it is secreted in the ECM of cells on PEA+FN+rLTBP1, as previously shown by Miron et al.[35] Our immunostaining results showed that osteocalcin secreted by cells is deposited in the ECM (Figure 4N). Finally, we performed Alizarin red staining to evaluate the mineralization potential of PEA+FN+rLTBP1 surfaces and observed enhanced mineralization in the ECM, confirming the osteogenic potential of this platform (Figure 4O).

2.4. rLTBP1 Coating on Protein–Polymer Nanosurfaces Regenerates Nonhealing Radial Bone Defect in Mice

We next assessed the ability of rLTBP1-coated implant tubes to heal a critical-sized, nonhealing radial bone injury in a murine model. For this, cylindrical-shaped, porous polyimide sleeves were cut into 4 mm long pieces and coated with a thin PEA layer (≈120 nm).[30] Sequential coating with FN and rLTBP1 at two different doses was then performed for treatment groups (5 or 50 μg mL^{-1} rLTBP1), whereas 3 μL collagen hydrogel loaded with hBMP-2 (human bone morphogenetic protein-2) at 75 μg mL^{-1} was pipetted into the porous sleeves to be used as positive control as it completely bridges the proximal and distal ends of the 2.5 mm bone injury.[29] An image of the porous implant tube is shown in Figure S10 (Supporting Information). We have previously reported that PEA+FN surfaces coated with growth factors (e.g., BMP-2) can heal critical-sized bone defects.[29] Implants coated with PEA alone fail to completely regenerate bone injuries and result in statistically lower bone volume fraction.[29,30]

The BMP-2-loaded collagen hydrogel produced complete bone regeneration (bridging of the defect), justifying its suitability as a positive control (**Figure** 5A,B). 50% and 40% of implant tubes coated with PEA+FN+rLTBP1 at 5 and 50 μg mL^{-1} concentrations, respectively, also completely bridged the bone defect. Nonbridged defects had an average gap length of <0.2 mm in both rLTBP1 groups, indicating that >90% of the defect had been bridged in this group (Figure 5C). Despite the variations in complete bridging between rLTBP1 groups and the positive control, bone volume, thickness, and tissue mineral density were comparable between all groups (Figure 5D–F). It is noteworthy that rLTBP1-containing implants that stimulate osteoinduction are in 2D scaffolds, but display bone regeneration potential that is comparable to a 3D hydrogel scaffold. The micro-computed-tomography (μCT) scans of all bone defects in positive control as well as treatment groups are shown in Figure S11 (Supporting Information).

Histological analysis confirmed these findings, showing the presence of fully developed, mineralized tissue. Bone marrow encased within cortical bone was present within all three injury groups, indicating a successful regenerative process, producing fully functional bone tissue that is matured and vascularized. In addition, both rLTBP1 concentrations (5 and 50 μg mL^{-1}) induced osteoinduction. We propose that the slightly lower potency of 5 μg mL^{-1} rLTBP1 is a dose-dependent effect, and that the differences in complete bridging between the experimental and positive control groups might be a dose-dependent and/or temporal effect (Figure 5C–E). Indeed, the BMP-2 containing positive control completely regenerated the bone defect, but, also led to fusion of the radius and ulna (Figure 5B). This nonsite-specific bone growth is evidence of excessive (heterotopic) bone formation and can result, among other side effects, in reduced range of motion. Heterotopic bone formation is possibly the result of using an active growth factor (BMP-2), as opposed to an inactive growth factor (rLTBP1) that is subsequently activated at the site of interest, thus controlling bone growth.

The use of active growth factors to stimulate bone regeneration[36] is inherently flawed because these multifunctional biomolecules play crucial roles in normal and abnormal physiological functions of the body. As such, it is essential to control the extent of their activation. To achieve this, different scaffold materials are being experimented with to limit the release of active growth factors, but have yet to be translated into the clinic as bone regenerative therapies.

In this study, we addressed the key limitations of using active growth factors to stimulate bone regeneration by utilizing a

confirming the knockdown efficiency of siRNA at protein level. E) Phospho Smad 2/3 levels on immunoblots. Smad 2/3 was highly phosphorylated in cells seeded on PEA+FN+rLTBP1, confirming the activation of TGF-β1 signaling pathway. F) Immunostaining of F-actin and p-MLC2 without or with 10 μM of Rock inhibitor, Y-27632. Rock inhibition disrupted F-actin stress filaments and reduced p-MLC2 immunostaining. Scale bar = 50 μm. G) Colocalization of integrin β1 and LAP as observed via immunostaining, without or with 10 μM of Rock inhibitor, Y-27632. Rock inhibition disrupted β1/LAP colocalization. Scale bar = 50 μm. H,I) Rock inhibition alters (H) p-MLC2 and p-MYPT1 protein levels ($N = 1$), and (I) TGF-β1 protein levels ($N = 2$), as shown by Western blotting. "N" refers to the number of biological replicates. J) RT-qPCR analysis of osteogenic biomarkers. Cells seeded on PEA+FN+rLTBP1 expressed significantly higher levels of the *BGLAP* (osteocalcin), *SPP1* (Secreted Phosphoprotein 1, osteopontin) and *Runx-2* genes, which all decreased on TGF-β1 siRNA-mediated knockdown, confirming that they are transcriptionally regulated by TGF-β1. Gene expression levels of *TGFB1* also decreased, confirming the siRNA knockdown efficiency. Gene expression on different surfaces was normalized to that on PEA-only coated surfaces ($n = 3$, Shapiro–Wilk normality test, followed by one-way ANOVA with Tukey's multiple comparison test). K) Immunoblots showing osteopontin protein levels after day 7 of culture on different surfaces. GAPDH was used as a loading control and PEA as the reference sample for quantification. L,M) RT-qPCR analysis of osteogenic biomarker and *TGFB1* expression after 14 and 28 days, respectively, on PEA, FN, and FN+*LTBP1* surfaces. Gene expression on different surfaces was normalized to that on PEA-only coated surfaces ($n = 3$, Shapiro–Wilk normality test, followed by one-way ANOVA with Tukey's multiple comparison test). N) Immunostaining of osteocalcin after 28 days in cell cultured on PEA, FN, or FN+*LTBP1* surfaces. Osteocalcin was secreted into the ECM after 28 days. Scale bar = 100 μm. O) Alizarin Red staining after 28 days of cell culture on different surfaces. Purple staining in the ECM, indicative of mineralization, was observed on PEA+FN+rLTBP1 surfaces Scale bar = 25 μm.

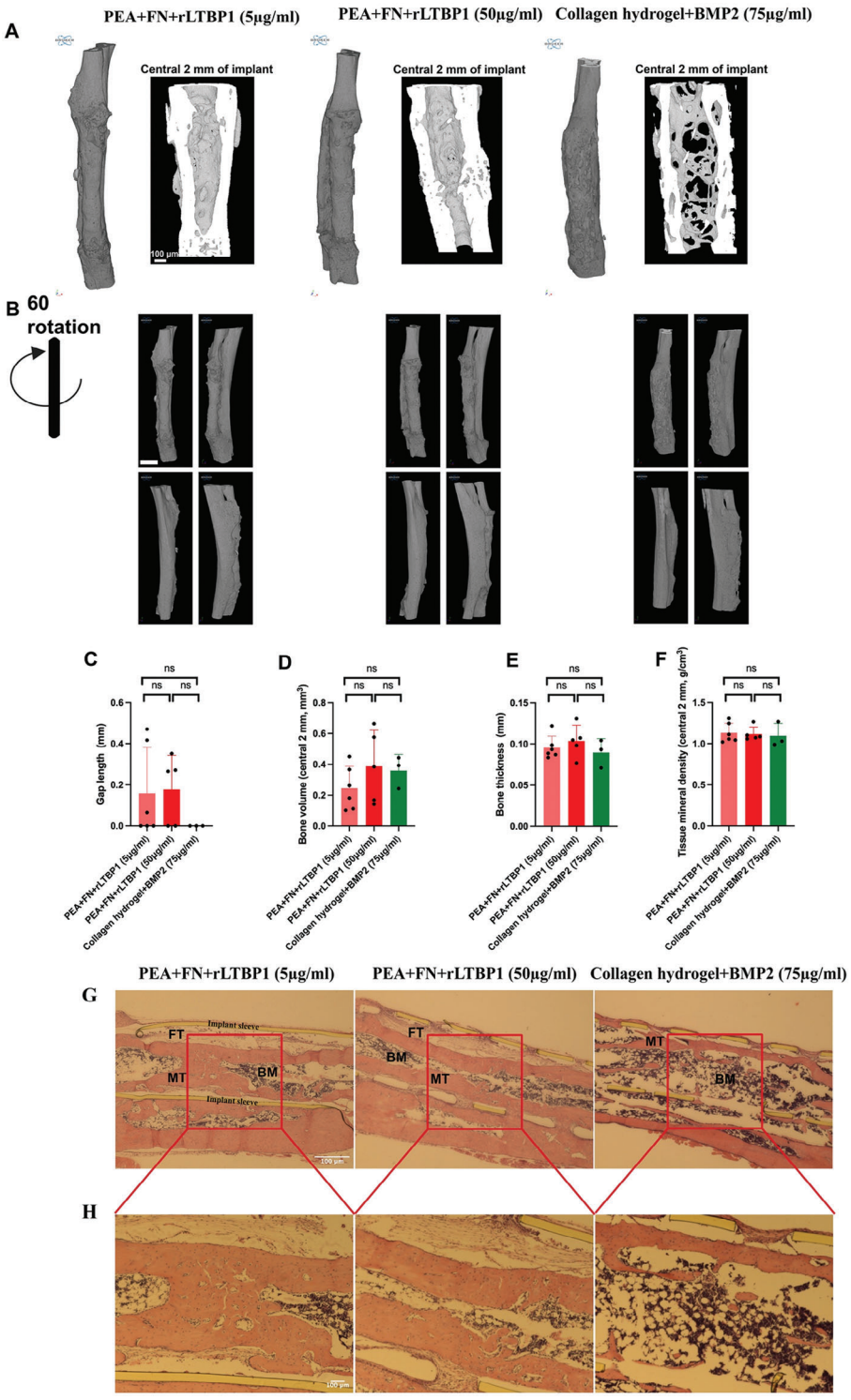

Figure 5. Promoting capture of TGF-β1 to rLTBP1 peptide-coated nanosurfaces promotes bone regeneration in a critical-sized bone defect in mice. A) (Left) 3D reconstruction of μCT images showing the induced radial bone defect, and (right) the central 2 mm of the implant area. Implants were loaded with 5 or 50 μg mL^{-1} of rLTBP1, or with collagen hydrogel containing BMP-2 (positive control). White and gray areas highlight the newly formed bone. The gray areas indicate interior bone surfaces. Scale bar = 100 μm. B) Images of 3D reconstructions after 60° clockwise rotation. Four representative images correspond to 0°, 60°, 240°, and 300° rotation of the μCT image. The images show bone regeneration as observed from different angles and highlight potential fusion between radius and ulna. Scale bar = 50 μm .C–F) Quantitative analysis of bone regeneration via assessment of gap length, bone volume in the central 2 mm of the implant tube, bone thickness, and tissue mineral density in the central 2 mm of the implant tube, for each implant type. $n = 3$ for positive control (collagen hydrogel+BMP-2), $n = 6$ for PEA+FN+rLTBP1 at 5 μg mL^{-1}, and $n = 5$ for PEA+FN+rLTBP1 at 50 μg mL^{-1}. Normality was assessed using Shapiro–Wilk test, followed by statistical analysis of quantitative data using ANOVA with multiple comparison's

recombinant fragment of *LTBP1* (rLTBP1). Our results show that rLTBP1 binds to the growth factor and integrin-binding domains of FN to facilitate the on-site and on-demand release of TGF-β1 from LAP, via mechanical means (Figure 2E–G). Although fibronectin use is limited in a clinical context, we show that rLTBP1 stimulates cells to produce their own FN in large amounts, which can serve as a scaffold for growth factor storage at the site of a bone defect for regeneration (Figure 3E,F). Although the combination of PEA+FN+rLTBP1 produces the highest TGF-β1 activation in our in vitro models, rLTBP1 also displays high levels of stability when immobilized on surfaces that are not coated with PEA or FN, indicating the potential of rLTBP-only coated implants for use in bone regeneration (Figure 1I,J). In our proof-of-concept, in vivo experiments, 2D implant tubes coated with rLTBP1 stimulated bone regeneration to a similar extent to that observed for the positive, 3D BMP-2-laden collagen hydrogel controls. This highlights the potential of rLTBP1 as a substitute for BMP-2 in bone regenerative therapies (Figure 5C–F). The engineered platform we report here might also work more efficiently as a 3D model.

In conclusion, we have shown that we can promote capture of inactive growth factor molecules onto implants to undergo site-specific, integrin-mediated, mechanical activation, providing an alternative to the use of active growth factors in bone regenerative therapies and overcoming a major hurdle in translational medicine.

3. Experimental Section

Morphological Characterization of Fibronectin Coating: AFM was performed to visualize fibronectin nanonetworks on PEA-coated surfaces. 13 mm circular glass coverslips were cleaned by sonicating in ethanol for 30 min and allowed to dry followed by coating with PEA. Substrates were coated with PEA using a custom-built capacitively coupled plasma reactor following the protocol described elsewhere.[37] Coverslips were then coated with FN (20 µg mL^{-1}) for 10 min at room temperature and first washed thrice with Dulbecco's phosphate-buffered saline (DPBS) followed by a final deionized wash.

SEM was also performed to study morphology of fibronectin coating on PEA-coated surfaces. Cleaned, PEA-coated circular 13 mm glass coverslips were coated with FN (20 µg mL^{-1}) for 1 h, washed thrice using DPBS, and fixed using 2.5% glutaraldehyde (FisherScientific, Cat: 10269452) for 30 min in dark. Samples were washed thrice using DPBS and counterstained using 1% osmium tetraoxide (FisherScientific, Cat: 10616881) for 15 min in dark. Surfaces were washed thrice using DPBS and critical point drying was performed using hexamethyldisilazane (Merck, Cat: 440191) for 30 min in dark. Samples were mounted onto stubs, coated with gold (20 nm thickness), and imaged using field-emission SEM (Carl Zeiss). Working distance of the instrument was set at 4.7 mm and FN nanonetworks were imaged at an accelerating voltage of 5 kV at different magnifications. All experimental steps were performed at room temperature.

Quantification of Fibronectin and rLTBP1 Adsorption: Circular 13 mm cleaned glass coverslips were coated with PEA. PEA-coated or uncoated coverslips were then coated with 50, 20, or 10 µg mL^{-1} FN (Biotechne, Cat: 1918-FN-02M) and washed thrice using DPBS. After 1 h, supernatant was collected and the amount of FN adsorbed was measured using micro-BCA protein assay kit (ThermoFisher Scientific, Cat: 23235) following manufacturer's instructions. An eight-point standard curve with twofold serial dilutions starting with 20 µg mL^{-1} FN concentration was plotted. FN concentration adsorbed on surfaces was calculated using Equation (1) and expressed as surface area density

$$\begin{aligned}&\text{Concentration of FN or } \textit{LTBP}1 \text{ adsorbed}\\&= \text{Concentration of FN or } \textit{LTBP}1 \text{ in aliquot placed on coverslip}\\&- \text{Concentration of FN or } \textit{LTBP}1 \text{ in the supernatant}\end{aligned} \quad (1)$$

After FN adsorption (20 µg mL^{-1}), surfaces were washed thrice with DPBS and then coated with 500 ng mL^{-1} concentration of rLTBP1 for 1 h at room temperature. The concentration of rLTBP1 absorbed was calculated using the same methodology used for FN concentration and expressed as surface area density (ng cm^{-2}).

Availability of Growth-Factor- and Integrin-Binding Domains of Fibronectin: PEA-coated or uncoated 96-well tissue-culture-treated plates were first coated with FN at 20 µg mL^{-1} concentration, washed thrice using wash buffer (0.05% Tween-20 in DBPS), and then blocked using 1% bovine serum albumin (BSA) for 30 min at room temperature. The surfaces were then incubated with primary P5F3 antibody (mouse monoclonal, Santa Cruz, Cat: sc-18827, 1:90) which bound to growth factor-binding FN(III_{12-14}) domain or HFN7.1 antibody (mouse monoclonal, developmental studies hybridoma bank, 1:330) which bound to integrin-binding domain FN(III_{9-10}) for 1 h at room temperature. The surfaces were then washed thrice using wash buffer and then incubated in horseradish-peroxidase (HRP)-conjugated secondary antibody (polyclonal, goat anti-mouse, ThermoFisher Scientific, Cat: 62-6520, 1:5000) diluted in 1% BSA for 1 h at room temperature. Surfaces were washed thrice using wash buffer and then incubated with substrate solution (Biotechne, Cat: DY999) for 20 min in dark followed by addition of stop solution (Biotechne, Cat: DY994). Plate absorbance was measured at 450 and 540 nm. Wavelength correction was performed by subtracting absorbance at 570 nm from that of 450 nm and the availability of domains was expressed as relative absorbance (a.u.).

Characterization of Fibronectin+rLTBP1 Interaction: The interaction between FN and rLTBP1 was investigated using coimmunoprecipitation. Fibronectin (2 mg mL^{-1}) and rLTBP1 (200 µg mL^{-1}) were gently mixed and incubated at room temperature for 1 h. Simultaneously, Dynabeads Protein G magnetic beads (ThermoFisher Scientific, Cat: 10003D) were first washed thrice in wash buffer (0.01% Tween-20 in DPBS) and then conjugated with fibronectin antibody (Mouse monoclonal, Proteintech group, Cat: 66042-1-Ig) by incubating the beads–antibody mixture in PBS for 20 min at 4 °C on rotary shaker. Bead–antibody complex was washed thrice in wash buffer and then incubated with FN+rLTBP1 mixture for 3 h at 4 °C on rotary shaker. Bead–antibody–protein complex was separated using Dynamag-2 magnet (ThermoFisher Scientific, Cat: 12321D) and washed thrice using wash buffer to remove unbound FN or rLTBP1. The complex was eluted in Bolt LDS (lithium dodecyl sulphate) sample buffer (ThermoFisher Scientific, Cat: B0007, final concentration 2×) containing Bolt sample reducing agent (ThermoFisher Scientific, Cat: B0009) at a final concentration of 1×. The final elute volume was fixed at 50 µL, loaded on a 4–12% Bolt Bis-Tris gel (ThermoFisher Scientific, Cat: NW04122BOX) and sodium dodecyl sulfate–polyacrylamide gel electrophoresis (SDS-PAGE) was performed by running the gel at 200 V for 30 min in MOPS NuPage running buffer (ThermoFisher Scientific, Cat: NP0001).

Proteins were transferred onto PVDF (Polyvinylidene difluoride) membrane (Merck, Cat: IEVH85R) in Bolt transfer buffer containing 20% methanol (ThermoFisher Scientific, Cat: BT00061) at 20 V, 160 mA for 70 min in a cooled environment. Membrane was first washed thrice in dH_2O to remove methanol then blocked using 5% BSA for 1 h at room temperature and probed using fibronectin and *LTBP1* antibody (rabbit polyclonal,

test (D, E) or using Kruskal–Wallis with Dunn's multiple comparisons test (C, F). G,H) Hematoxylin and eosin (H&E) staining of implants after 8 weeks of implantation. FT, MT, and BM refer to fibrous tissue, mineralized tissue, and bone marrow, respectively. Implant sleeve labeling shows top and bottom outline of implant tube with bone regeneration within.

Proteintech group, Cat: 26855-1-AP) diluted in 5% BSA for overnight at 4 °C. The following day, membranes were first washed thrice using Tris-buffered saline containing 0.1% Tween-20 (TBST) and then incubated with Clean-Blot IP detection reagent (ThermoFisher Scientific, Cat: 21230, 1:200) which detected only denatured antibodies. This was done to avoid or minimize signal from native antibody (antifibronectin). Protein bands were visualized using a chemiluminescent substrate (ThermoFisher Scientific, Cat: 34580). Beads alone and native antifibronectin antibody alone were used as negative controls.

Characterization of rLTBP1 Interaction with FN(III_{12-14}) and FN(III_{9-10}) Domains: Coimmunoprecipitation was performed to study if rLTBP1 interacted and bound with growth-factor- and integrin-binding domains of FN. FN(2 mg mL^{-1}) was first incubated with P5F3 or HFN7.1 antibodies for 1 h at room temperature to allow blocking of FN(III_{12-14}) and FN(III_{9-10}) domains, respectively. The source and clonality of both antibodies were mentioned above. rLTBP1 (200 µg mL^{-1}) was then incubated with the FN-P5F3 or FN-HFN7.1 mixture for 1 h at room temperature. Coimmunoprecipitation was performed using FN antibody following the methodology described above. Briefly, magnetic beads were first conjugated with FN antibody and the bead–antibody complex was then incubated with protein–antibody–rLTBP1 mixture. SDS-PAGE and western blotting were performed using the methodology described above. Beads, native FN antibody, P5F3, or HFN 7.1 antibody alone were used as negative controls and FN+rLTBP1 mixture was used as a positive control. The decrease in rLTBP1 protein signal intensity was interpreted as decrease in its binding with FN due to blocking of FN(III_{12-14}) and FN(III_{9-10}) domains by respective antibodies. The decrease in signal intensity was quantified with respect to intensity of positive control (FN+rLTBP1) using image J.

Cell Culture: hMSCs (PromoCell, Cat: C-14090) were used for all experiments in this study. Cells were cultured in Dulbecco's Modified Eagle's Media (Sigma, Cat: D5671) supplemented with 10% fetal bovine serum (FBS, Signa, Cat: 26010), 0.4% penicillin/streptavidin, nonessential amino acids (Gibco, Cat: 11140-35), L-Glutamine (Gibco, Cat: G7513), sodium pyruvate (Sigma, Cat: S8636), and 0.5% amphotericin B (Gibco, Cat: 15290-026). Cell cultures were incubated in 5% CO_2 atmosphere in a humidified incubator. Cells at passage ≤ 3 were used for all experiments and for first 3 h of all experiments, cells were cultured in media containing 1% FBS.

Gene Expression Profiling: hMSCs were seeded at a density of 2000 cells cm^{-2} for different time periods (7, 14, or 28 days) and relative change in *LTBP1*, TGF-β1, Smad 2, Smad 3, osteocalcin, osteopontin, osteonectin, *Runx-2* gene expression was studied using quantitative RT-qPCR. 6-well tissue-culture-treated plates were first coated with PEA and UV-sterilized followed by coating with FN (20 µg mL^{-1}) for 1 h. The wells were then washed thrice using DPBS and coated with rLTBP1 (500 ng mL^{-1}) for 1 h. Finally, wells were washed thrice using DPBS and cells were seeded in media containing 1% FBS. After 3 h, the media was aspirated, replaced with complete media containing 10% FBS and cells were allowed to grow for predetermined time periods. Media was changed every 2 to 3 days. Total RNA (tRNA) was extracted using Trizol (ThermoFisher, Cat: A33250), precipitated using isopropanol, and washed thrice using 80% ice-cold ethanol. tRNA pellet was dissolved in 20 µL nuclease-free water (ThermoFisher, Cat: AM9938) and quantified using Nanodrop 2000. $OD_{260/280}$ and $OD_{260/230}$ (optical density) were measured to determine the purity or presence of organic contaminants in the tRNA. 1 µg RNA was used for reverse transcription. First, DNA contamination was removed using ezDNase following manufacturer's instructions followed by reverse transcription using SuperScript IV reverse transcriptase system (ThermoFisher Scientific, Cat: 12595025). Gene of interest (GOI) expression on different surfaces were quantified by PCR using PowerUp SYBR Green Master Mix (ThermoFisher, Cat: A25741) containing ROX (6-carboxyl-X-Rhodamine) as passive reference dye. Reaction mixture containing cDNA template (complementary deoxyribonucleic acid), forward and reverse GOI primers, and SYBR green dye in a total reaction mixture of 10 µL was run in Fast 96-Well plated (Applied Biosystems, Cat: 4346907) on 7500 Real-Time PCR system machine (Applied Biosystems) in Fast mode. Relative gene transcript levels were calculated using ΔΔCt method and glyceraldehyde 3-phosphate dehydrogenase (GAPDH) was used as a housekeeping gene. Finally, relative fold change was expressed as $2^{-(\Delta\Delta Ct)}$ and the data were represented as mean with standard deviations.

Protein Analysis Using Western Blotting: Nunc 100 × 150 mm dishes (ThermoFisher Scientific, Cat: 150350) were coated with PEA, UV-sterilized, and coated with FN and rLTBP1 as described above. Cells were seeded at a density of 4000 cells cm^{-2} for 7 days. Media was changed on day 3 and day 5. After predetermined time period, cells were washed with ice-cold DPBS, scrapped, and pelleted by centrifugation at 1500 RPM for 5 min. Cell pellet was lysed in radioimmunoprecipitation assay buffer containing protease and phosphatase inhibitors (ThermoFisher Scientific, Cat: 78442) at 1× final concentration. Protein was extracted by centrifugation at 13 200 RPM for 30 min at 2 °C. Cell pellet was discarded and supernatant was transferred into a new Eppendorf. Protein was quantified using BCA assay kit (ThermoFisher Scientific, Cat: 23227) and equal amount of protein was loaded onto 4–12% Bolt Bis-Tris gels and SDS-PAGE was performed at 200 V for 35 min. Proteins were transferred onto PVDF membranes using methodology described above and blocked in 5% nonfat dry milk (NFDM, Santa Cruz, Cat: sc-2324) for 1 h at room temperature. Membrane was incubated overnight with protein-specific antibodies diluted in 5% NFDM at 2 °C. The following day, PVDF membrane was first washed thrice using TBST and then incubated with the corresponding HRP-conjugated secondary antibody diluted in 5% NFDM for 1 h at room temperature. Proteins were visualized using a chemiluminescent substrate. GAPDH or α-Tubulin was used as a loading control. Protein bands were quantified using densitometry in ImageJ (National Institute of Health, USA). All reagents used for western blotting were same as described above.

Antibodies: The following antibodies were used for western blotting and immunofluorescence: Smad 2/3 antibody (Rabbit polyclonal, Cell Signaling Technology, Cat: 3102S), phospho Smad 2/3 (Rabbit monoclonal, Cell Signaling Technology, Cat: 8828S), osteopontin (Rabbit polyclonal, Abcam, Cat: ab8448), osteocalcin (Rabbit polyclonal, Proteintech group, Cat: 23418-1-AP), LAP (mouse monoclonal, ThermoFisher Scientific, Cat: 16-9823-82), TGF-β1 (rabbit polyclonal, Proteintech group, Cat: 21898-1-AP), GAPDH (mouse monoclonal, Proteintech group, Cat: 60004-1-Ig), α-Tubulin (mouse monoclonal, Abcam, Cat: ab7291), integrin β1 (Rabbit polyclonal, Proteintech group, Cat: 12594-1-AP), *LTBP1* (rabbit polyclonal, Proteintech group, Cat: 26855-1-AP), p-MLC2 (rabbit polyclonal, Cell Signaling Technology, Cat: 3674), and p-MYPT1 (Rabbit polyclonal, Cell Signaling Technology, Cat: 4563).

Immunofluorescence: 4-well chamber slides (ThermoFisher Scientific, Cat: 154917PK) were first coated with PEA, UV-sterilized, and then coated with FN and rLTBP1. Cells were seeded at a density of 4000 cells cm^{-2} for 7 days. On days 3 and 5, 70% of the media was removed and replaced with fresh media. Care was taken to prevent the wells from drying. After predetermined time period, media was aspirated, and cells were gently washed once with prewarmed DPBS and then fixed in 4% formaldehyde for 15 min at room temperature. Wells were gently washed thrice for 5 min each with DPBS and cells were then permeabilized using 0.05% Triton X-100 for 15 min at room temperature. Cells were blocked using 3% BSA for 1 h at room temperature and then incubated with primary antibodies diluted in 3% BSA for overnight in a humidified chamber. Care was taken to add ample antibody solution to prevent wells from drying overnight. The following day, cells were first gently washed thrice for 5 min using PBS and the incubated with Alexa Fluor 568-conjugated goat anti-rabbit (ThermoFisher, Cat: A-11011, 1:500) or Alexa Fluor 647-conjugated donkey anti-mouse (ThermoFisher, Cat: A-31571, 1:500) secondary antibodies diluted in 2% BSA for 1 h at room temperature in dark. Finally, cells were washed thrice using DPBS and mounted using mounting media (ThermoFisher, Cat: P36962) and inverting a 0.17 mm coverslip onto the glass slide. Samples were allowed to dry overnight, edges were sealed using nail polish, and proteins were imaged using a confocal microscope (Zeiss LSM 880 confocal microscope with Airyscan) at 40× and 63× magnifications. Primary antibodies used for colocalization experiments were raised in different species (e.g., mouse and rabbit) and the chosen secondary antibodies were conjugated to different fluorophores (e.g., Alexa Fluor 568 and Alexa Fluor 647).

Coimmunoprecipitation for Studying Protein–Protein Interactions: Cells were seeded at a density of 2000 cells cm^{-2} on PEA-coated 10 cm culture dishes for 7 days. After predetermined time period, cells were washed once with ice-cold DPBS, scraped on ice using a cell scrapper, and pelleted by centrifugation at 1500 RPM for 5 min. Cells were lysed using immunoprecipitation lysis buffer (ThermoFisher Scientific, Cat: 87787) containing protease and phosphatase inhibitors and protein was extracted by centrifugation at 13 200 RPM for 30 min at 2 °C. Protein was quantified using BCA assay. Equal volume of primary antibody (latency associated peptide) was added to equal amount of protein lysates and lysates were precleared by incubation at 4 °C overnight on a rotary shaker. The following day, Dynabeads Protein G was washed thrice in wash buffer and mixed with protein lysate–antibody mixture for 20 min at 4 °C on a rotary shaker. Magnetic bead–antibody–protein complex was isolated using Dynamag-2, then mixed with Bolt LDS sample buffer with a final concentration of 2× and Bolt sample reducing agent with a final concentration of 1×. The total volume was brought to 40 µL using dH_2O. The mixture was incubated at room temperature for 30 min to allow protein elution. SDS PAGE and western blotting were performed as described above. Clean-Blot immunoprecipitated (IP) detection reagent was used for detection of IP and probed antibodies to avoid interference of proteins bands from denatured IP antibody.

RNA Interference: TGF-β1 gene knockdown was performed in 6-well or 10 cm culture dishes. Cells were seeded at a density of 2000 cells cm^{-2}. RNAi (Ribonucleic acid interefence) was performed using stem transfection reagent (ThermoFisher Scientific, Cat: STEM00003) following manufacturer's instructions. siRNA was purchased from ThermoFisher Scientific (Cat: 4390824) and used at a final concentration of 40 nM. Briefly, on day 3, when cells reached 50–70% confluency, complete media was aspirated and an appropriate volume of Opti-MEM reduced serum media was added to wells (ThermoFisher Scientific, Cat: 31985070). siRNA diluted in Opti-MEM was added to wells and incubated overnight. The following day, media containing siRNA was aspirated, replaced with complete media and cells were allowed to grow till day 7.

Alizarin Red Staining: Alizarin red solution was prepared by dissolving Alizarin red mono sodium salt (Sigma, Cat: 1062780025) in dH_2O. The solution was well-mixed and the pH adjusted to 4.2. Cells were cultured on uncoated or PEA-coated surfaces for 21 days, and then fixed using 4% formaldehyde for 10 min at room temperature and washed thrice using DPBS. Alizarin red solution was then added and incubated with cells for 15 min at room temperature. Cells were washed several times with dH_2O to remove excess stain and imaged using an optical microscope.

Rock Inhibition: Rock inhibition was performed to assess the role of integrins in TGF-β1 activation. Cells were first cultured on PEA+FN+rLTBP1-coated surfaces for 5 days. On day 6, complete media was aspirated and replaced with Opti-MEM reduced serum media to sync cell cycle. On day 7, Rock inhibitor (Y-27632, Tocris, Cat: 1254) was added to the media and cells were incubated for 4 h. Immunostaining and western blotting were performed using the protocols described above.

Nonunion Radial Bone Segmental Defect Murine Model: The in vivo experiments were conducted under the Animals (Scientific Procedures) Act 1986 (ASPeL project license PP5891831). All the research performed complied with ethical regulations approved by the University of Glasgow's ethical committee.

Implant Preparation: Perforated, porous, polyimide sleeves (4 mm length) were coated with a thin layer (≈120 nm thickness) of plasma-polymerized PEA. Implants were left in continuous vacuum extraction to remove any potential monomer traces, and then sterilized with UV light. Then, fibronectin (20 µg mL^{-1}) and rLTBP1 (5 or 50 µg mL^{-1}) were sequentially adsorbed on the sleeve surface by incubating the treated tubes in the corresponding protein solution. Sleeves filled with 3 µL of collagen hydrogel loaded with hBMP-2 growth factor (75 µg mL^{-1}) were used as positive control.

Radial Bone Segmental Defect Surgery: C57B1/6J male and female mice (8–10 weeks old, Charles Rivers) were anesthetized using isoflurane gas, and provided with a dose of buprenorphine and carprofen for pain relief. The right forelimb was shaved and swabbed with povidone-iodine. Then, an incision on the skin was made along the forearm, and the soft tissue was carefully separated by blunt dissection using a periosteal elevator to expose the radial bone. A 2.5 mm bone defect was created in the center of the radius using a custom-made parallel double-bladed bone cutter, without disturbing the ulna. The implant was placed into the defect by fitting the tube over the proximal and distal ends of the radial defect. Then, the soft tissue was repositioned and the wound was closed using degradable sutures. Mice were monitored after surgery for signs of distress, movement, and weight loss. 6 mice (3 males and 3 females) were used per experimental condition. Eight weeks after surgery, the mice were sacrificed, and the bone samples were explanted, fixed in 4% paraformaldehyde, and immersed in 70% ethanol for further analysis.

µCT for Assessing New Bone Formation: Mouse radial defects were µCT scanned at an isotropic voxel size of 3 µm, using the Skyscan 1172 scanner (80 kVp/100 µA Hamamatsu X-ray, Bruker, Kontich, Belgium). The following scan parameters were used for all samples: 60 kVp tube voltage, 100 µA tube current, 1750 ms exposure time, 0.3° rotation step size for a total of 180°, with frame averaging set to 2, and a 0.5 mm thick aluminum filter placed in front of the X-ray source. Projection images were reconstructed using Skyscan NRecon software (Version 1.6.9.18, Bruker). Reconstructed datasets were coregistered to ensure that all datasets were spatially aligned. Specifically, a representative dataset was selected and used as the reference standard dataset. This dataset was manually aligned such that the *z*-axis of the dataset corresponded with the long axis of the radius bone in DataViewer (Version 1.5.6.2, Bruker). Subsequently, all other datasets were rigidly coregistered against this reference dataset, in a semi-automated fashion using DataViewer.

To ensure measurement of only the newly formed bone within the critical sized defect, only the central 2 mm of the implant tube within a cylindrical volume of interest (VOI) with height of 2 mm, and diameter of 0.9 mm was analyzed in CTAnalyzer (Version 1.18.8.0, Bruker). A quantitative approach was taken to ensure reproducible VOI selection. Specifically, a survey of the 2D morphometric parameter bone area (BA) was conducted along the entire length of the radius bone, as per published methods.[38] This slice-by-slice analysis enabled the detection of the location two BA peaks, each corresponding to the formation of a bone callous at the location of the ends of the tube (Figure S10, Supporting Information). The midpoint between the two peaks was the center of the tube. The VOI was selected ±1 mm relative to the midpoint. Morphometric analysis was then performed on this VOI after binarization via a global threshold (85/255) and two despeckling operations; removal of white and black speckles (in 3D) less than 50 voxels in size, respectively. Outcome measures included bone volume and average bone thickness. The gap length between the two stumps was also measured using the slice-by-slice approach described above. Bone mineral density and tissue mineral density were determined following µCT scanning of two 2 mm diameter calibration hydroxyapatite rods (Bruker), of density 0.25 and 0.75 g cm^{-3}, respectively, with the same scanner settings described above.

Histological Analysis: Bone samples were decalcified using Krajian solution (citric acid/formic acid, Ricca) for 3 days, until they were soft and pliable. Samples were then rinsed and embedded in paraffin, and longitudinal sections (5 µm thickness) at different levels of the bone diameter were obtained using a microtome. These histological sections were stained with hematoxylin and eosin (H&E), then imaged with an EVOS FL microscope (4× and 10×, ThermoFisher, USA).

Statistics and Reproducibility: All experiments were triplicated, and the data were expressed as mean with standard deviations. For quantitative representation of data, the distribution was first assessed using Shapiro-Wilk test followed by statistical analysis using either one-way analysis of variance (ANOVA) with Tukey's multiple comparisons test when data displayed normal distribution or using Kruskal–Wallis test with Dunn's multiple comparisons test when data did not display normal distribution on GraphPad Prism (Version 9.5.0, Mac). The specific normality and statistical test employed for each quantitative data were described in their corresponding figure legends. The level of significance was set at 0.05. *p*-values ≤ 0.05, 0.01, and 0.001 were denoted with *, **, and ***, respectively. For in vivo experiments, the positive control group comprised of 3 and each treatment (PEA+FN+rLTBP1) comprised of 6 mice.

Supporting Information

Supporting Information is available from the Wiley Online Library or from the author.

Acknowledgements

This work was supported by the European Union's Horizon 2020 research and innovation programme (Grant No. 874889 – HEALIKICK) and the European Research Council AdG (Grant No. 101054728). C.G.-G. acknowledges support from the Engineering and Physical Sciences Research Council (Grant No. EPSRC NIA – EP/T000457/1). U.D. is grateful to his parents Dr. Viapak Dhawan and Dr. Neeru Bala, his wife Wei-Yun Su for support during challenging times in this work, and his teachers Prof. Guewha Steven Huang and Dr. Hsiao-hua Yu for teaching him valuable research lessons. The authors are grateful to Dr. Vineetha Jayawarna for help with XPS and AFM characterization of PEA and fibronectin coatings. The authors thank the UK national facility for photoelectron spectroscopy (Harwell XPS) for XPS characterization of samples. The authors gratefully acknowledge the Glasgow Imaging Facility for their support and assistance in this work. The authors acknowledge the Geoanalytical Electron Microscopy and Spectroscopy unit at the Glasgow University for the support and assistance with electron microscopy. Schematics in figures were created using BioRender.com. IBEC is member of CERCA Programme / Generalitat de Catalunya.

Conflict of Interest

The authors declare no conflict of interest.

Author Contributions

U.D. conceived the idea, designed and performed all in vitro experiments, analyzed the corresponding data, and assisted with the in vivo experiments. C.G.-G. designed and performed in vivo experiments, including histological analysis. J.A.W. and J.F.C.W. performed μCT imaging and analysis. U.D., J.A.W., and C.G.-G. analyzed in vivo data. M.J.D. acquired funding and provided intellectual input to paper preparation. M.S.-S. conceived the idea, acquired funding, coordinated the research, provided intellectual input to experimental design, and edited the paper. U.D. wrote the paper with input from J.A.W., P.C., C.G.-G., M.J.D., and M.S.-S. All authors read and approved the final version of the paper.

Data Availability Statement

The data that support the findings of this study are available from the corresponding author upon reasonable request.

Keywords

bone regeneration, fibronectin, growth factors, *LTBP1*

Received: October 16, 2023
Revised: January 13, 2024
Published online: February 2, 2024

[1] Z. T. Chen, D. L. Yi, X. B. Zheng, J. Chang, C. T. Wu, Y. Xiao, *J. Mater. Chem. B* **2019**, *7*, 3319.
[2] K. Hashimoto, T. Kaito, M. Furuya, S. Seno, D. Okuzaki, J. Kikuta, H. Tsukazaki, H. Matsuda, H. Yoshikawa, M. Ishii, *Sci. Rep.* **2020**, *10*, 4751.
[3] K. R. Garrison, I. Shemilt, S. Donell, J. J. Ryder, M. Mugford, I. Harvey, F. Song, V. Alt, *Cochrane Database Syst. Rev.* **2010**, *6*.
[4] E. A. Bayer, R. Gottardi, M. V. Fedorchak, S. R. Little, *J. Controlled Release* **2015**, *219*, 129.
[5] J. Tazaki, M. Murata, T. Akazawa, M. Yamamoto, K. Ito, M. Arisue, T. Shibata, Y. Tabata, *Biomed. Mater. Eng.* **2009**, *19*, 141.
[6] B. Hinz, *Matrix Biol.* **2015**, *47*, 54.
[7] A. Walker, J. E. Turnbull, J. T. Gallagher, *J. Biol. Chem.* **1994**, *269*, 931.
[8] R. Pankov, K. M. Yamada, *J. Cell Sci.* **2002**, *115*, 3861.
[9] F. Klingberg, G. Chau, M. Walraven, S. Boo, A. Koehler, M. L. Chow, A. L. Olsen, M. Im, M. Lodyga, R. G. Wells, E. S. White, B. Hinz, *J. Cell Sci.* **2018**, *131*, jcs201293.
[10] F. B. Lin, X. D. Ren, Z. Pan, L. Macri, W. X. Zong, M. G. Tonnesen, M. Rafailovich, D. Bar-Sagi, R. A. F. Clark, *J. Invest. Dermatol.* **2011**, *131*, 84.
[11] M. M. Martino, P. S. Briquez, A. Ranga, M. P. Lutolf, J. A. Hubbell, *Proc. Natl. Acad. Sci. USA* **2013**, *110*, 4563.
[12] M. M. Martino, F. Tortelli, M. Mochizuki, S. Traub, D. Ben-David, G. A. Kuhn, R. Muller, E. Livne, S. A. Eming, J. A. Hubbell, *Sci. Transl. Med.* **2011**, *3*, 100ra89.
[13] M. M. Martino, J. A. Hubbell, *FASEB J.* **2010**, *24*, 4711.
[14] J. Zhu, S. Angelov, I. A. Yildirim, H. Wei, J. H. Hu, M. W. Majesky, F. V. Brozovich, F. Kim, D. A. Dichek, *Arterioscler., Thromb., Vasc. Biol.* **2021**, *41*, 1956.
[15] T. C. Brionne, I. Tesseur, E. Masliah, T. Wyss-Coray, *Neuron* **2003**, *40*, 1133.
[16] G. Du, X. Cheng, Z. Zhang, L. Han, K. Wu, Y. Li, X. Lin, *Front. Genet.* **2021**, *12*, 759596.
[17] G. Chen, C. Deng, Y. P. Li, *Int. J. Biol. Sci.* **2012**, *8*, 272.
[18] A. B. Kulkarni, C. G. Huh, D. Becker, A. Geiser, M. Lyght, K. C. Flanders, A. B. Roberts, M. B. Sporn, J. M. Ward, S. Karlsson, *Proc. Natl. Acad. Sci. USA* **1993**, *90*, 770.
[19] J. Xu, J. Liu, Y. Gan, K. Dai, J. Zhao, M. Huang, Y. Huang, Y. Zhuang, X. Zhang, *J. Bone Miner. Res.* **2020**, *35*, 167.
[20] S. Maeda, M. Hayashi, S. Komiya, T. Imamura, K. Miyazono, *EMBO J.* **2004**, *23*, 552.
[21] Z. Yu, Y. Li, Y. Wang, Y. Chen, M. Wu, Z. Wang, M. Song, F. Lu, X. Lu, Z. Dong, *Biosci. Rep.* **2019**, *39*.
[22] M.-N. Labour, M. Riffault, S. T. Christensen, D. A. Hoey, *Sci. Rep.* **2016**, *6*, 35542.
[23] J. L. Crane, X. Cao, *J. Clin. Invest.* **2014**, *124*, 466.
[24] L. Zhao, B. M. Hantash, *Vitam. Horm.* **2011**, *87*, 127.
[25] G. Jenkins, *Int. J. Biochem. Cell Biol.* **2008**, *40*, 1068.
[26] J. P. Annes, Y. Chen, J. S. Munger, D. B. Rifkin, *J. Cell Biol.* **2004**, *165*, 723.
[27] L. Buscemi, D. Ramonet, F. Klingberg, A. Formey, J. Smith-Clerc, J. J. Meister, B. Hinz, *Curr. Biol.* **2011**, *21*, 2046.
[28] S. L. Dallas, P. Sivakumar, C. J. Jones, Q. Chen, D. M. Peters, D. F. Mosher, M. J. Humphries, C. M. Kielty, *J. Biol. Chem.* **2005**, *280*, 18871.
[29] Z. A. Cheng, A. Alba-Perez, C. Gonzalez-Garcia, H. Donnelly, V. Llopis-Hernandez, V. Jayawarna, P. Childs, D. W. Shields, M. Cantini, L. Ruiz-Cantu, A. Reid, J. F. C. Windmill, E. S. Addison, S. Corr, W. G. Marshall, M. J. Dalby, M. Salmeron-Sanchez, *Adv. Sci.* **2019**, *6*, 1800361.
[30] V. Llopis-Hernandez, M. Cantini, C. Gonzalez-Garcia, Z. A. Cheng, J. Yang, P. M. Tsimbouri, A. J. Garcia, M. J. Dalby, M. Salmeron-Sanchez, *Sci. Adv.* **2016**, *2*, 1600188.
[31] C. Gonzalez-Garcia, M. Cantini, J. Ballester-Beltran, G. Altankov, M. Salmeron-Sanchez, *Acta Biomater.* **2018**, *77*, 74.

[32] L. Fontana, Y. Chen, P. Prijatelj, T. Sakai, R. Fassler, L. Y. Sakai, D. B. Rifkin, *FASEB J.* **2005**, *19*, 1798.
[33] M. G. Campbell, A. Cormier, S. Ito, R. I. Seed, A. J. Bondesson, J. Lou, J. D. Marks, J. L. Baron, Y. Cheng, S. L. Nishimura, *Cell* **2020**, *180*, 490.
[34] M. Shi, J. Zhu, R. Wang, X. Chen, L. Mi, T. Walz, T. A. Springer, *Nature* **2011**, *474*, 343.
[35] R. J. Miron, E. Hedbom, S. Ruggiero, D. D. Bosshardt, Y. F. Zhang, C. Mauth, A. C. Gemperli, T. Iizuka, D. Buser, A. Sculean, *PLoS One* **2011**, *6*, 23375.
[36] O. S. Nilsson, M. R. Urist, E. G. Dawson, T. P. Schmalzried, G. A. Finerman, *J. Bone Jt. Surg., Br. Vol.* **1986**, *68*, 635.
[37] Z. A. Cheng, A. Alba-Perez, C. Gonzalez-Garcia, H. Donnelly, V. Llopis-Hernandez, V. Jayawarna, P. Childs, D. W. Shields, M. Cantini, L. Ruiz-Cantu, A. Reid, J. F. C. Windmill, E. S. Addison, S. Corr, W. G. Marshall, M. J. Dolby, M. Salmeron-Sanchez, *Adv. Sci.* **2019**, *6*, 1800361.
[38] J. A. Williams, J. F. C. Windmill, K. E. Tanner, J. S. Riddell, S. Coupaud, *Bone Rep.* **2020**, *12*, 100233.